Effective Graphene Monopole and Its Application to Water Transport

Carlos Omeñaca Prado

December 2025

DECLARACIÓN DE DOMINIO PÚBLICO Y RENUNCIA DE DERECHOS

(CC0 1.0 Universal — Public Domain Dedication)

Yo, **Carlos Omeñaca Prado**, declaro que esta obra,
incluido su contenido técnico, dibujos, datos y anexos,
se entrega al **DOMINIO PÚBLICO GLOBAL**. Renuncio íntegramente
a cualquier derecho de autor o patente, y autorizo su uso,
reproducción y modificación sin restricción alguna.

Fecha: 3 de diciembre de 2025
Firma: Carlos Omeñaca Prado

PUBLIC DOMAIN AND RIGHTS WAIVER DECLARATION

(CC0 1.0 Universal — Public Domain Dedication)

I, **Carlos Omeñaca Prado**, hereby declare that this work,
including all its technical content, drawings, data and appendices,
is hereby released into the **GLOBAL PUBLIC DOMAIN**.
I completely and irrevocably waive any copyright or patent rights,
and authorize its use, reproduction and modification
without any restriction or limitation.

Date: December 3, 2025
Signature: Carlos Omeñaca Prado

GRAPHENE MONOPOLE PIECE

Carlos Omeñaca Prado

Año: 2025

Abstract

This work presents the first complete geometric, material, and operational design of an effective magnetic monopole generated through controlled symmetry breaking in a ferromagnetic core using a curved graphene patch, within the Quarkbase Cosmology framework. The model treats $B = \nabla \times A$ as the vorticity of the ether-like Ψ–field, allowing local nonclosure of vorticity lines when the medium is spatially inhomogeneous. By combining three coupled asymmetries—(i) an iron toroid with a 270°/90° cross-sectional discontinuity, (ii) a displaced sectoral coil, and (iii) a curvature-induced modification of graphene's $\alpha(\varepsilon)$ and Ψ-channel density—the device forces part of the internal vorticity to exit through a controlled region, producing a measurable pseudo-monopolar field.

The document provides the full fabrication parameters, theoretical justification from the Quarkbase equations, and experimental protocols to verify monopolar behavior through $B(r)$ profiles, angular anisotropy, front/back contrast, and discrete flux imbalance. A practical application is then developed: a water-pumping module in which the monopolar field establishes a sustained Ψ-pressure gradient capable of lifting water through a tube without mechanical pumps or moving parts. This enables continuous irrigation, filtration, and potable-water access in low-resource environments with minimal energy input.

All designs, equations, and engineering solutions presented here are released into the public domain (CC0) to ensure universal accessibility, non-patentability, and immediate applicability for humanitarian benefit.

Contents

1 Physical Basis of the Effective Monopole in the Quarkbase Framework 4
- 1.1 Fundamental premise: meaning of "monopole" in Quarkbase . . . 4
- 1.2 Mechanisms enabling vorticity "opening": graphene channels . . . 4
- 1.3 Why a standard toroid cannot, but a toroid with graphene can . . . 5
- 1.4 Justification using the internal equations of the theory . . . 6
- 1.5 Nature of the created object . . . 6

2 Geometry and Design of the Core with Curved Graphene Patch 7
- 2.1 Ferromagnetic core: shape and dimensions . . . 7
  - 2.1.1 Basic form . . . 7
  - 2.1.2 Asymmetric cross-section . . . 8
- 2.2 Displaced coil (coil offset) . . . 9
  - 2.2.1 Position . . . 9
  - 2.2.2 Electrical parameters . . . 9
- 2.3 Curved graphene patch . . . 9
  - 2.3.1 Patch geometry . . . 9
  - 2.3.2 Graphene type . . . 10
- 2.4 Housing and "monopole window" . . . 11
- 2.5 Distribution of B and symmetry breaking: Ψ-field dynamics . . . 11
- 2.6 Consistency with graphene-based predictions . . . 12

3 Core Excitation and Experimental Demonstration of Monopolar Behavior 12
- 3.1 Excitation modes of the device . . . 12
  - 3.1.1 DC mode . . . 12
  - 3.1.2 Low-frequency AC mode (1–50 kHz) . . . 13
  - 3.1.3 Longitudinal coupling mode: THz/MIR illumination of the patch . . . 13
- 3.2 Basic electrical setup . . . 14
- 3.3 Measurement protocol 1 — Radial profile $B(r)$ in front of the window . . . 14
- 3.4 Measurement protocol 2 — Angular pattern on a circular path . . . 15
- 3.5 Measurement protocol 3 — Front/back comparison . . . 16
- 3.6 Measurement protocol 4 — Discrete "magnetic Gauss test" . . . 17
- 3.7 Link to the fluid-pumping application (conceptual bridge) . . . 17

4 Water-Pumping Module Driven by the Effective Monopole 17
- 4.1 Physical principle of pumping in the Quarkbase framework . . . 18
- 4.2 Basic pump module: "Monopole at tube inlet" . . . 18
  - 4.2.1 Physical configuration . . . 18
  - 4.2.2 Step-by-step mechanism . . . 19
  - 4.2.3 Achievable lift height . . . 19
- 4.3 Variant 1 — Recirculation loop / continuous flow . . . 20
  - 4.3.1 Closed-loop setup . . . 20
  - 4.3.2 Immediate application . . . 20
- 4.4 Variant 2 — Assisted desalination/filtration module . . . 21
- 4.5 Variant 3 — Direct local irrigation module . . . 21
- 4.6 Consistency with the theory . . . 22

4.7 Impact on Hunger and Development . . . 22
4.7.1 Irrigation Capacity: Immediate Increase in Food Production . . . 22
4.7.2 Potable Water Access: Reduction of Water-Borne Disease . . . 23
4.7.3 Minimal Energy Requirement → Economic Independence . . . 23
4.7.4 Scalability: From One Household to Entire Communities . . . 24
4.7.5 Cumulative Effects on Human Development . . . 24

5 Complete Geometry and Design of the Ferromagnetic Core with Curved Graphene Patch 25
5.1 Ideal toroid: starting point and why it does NOT work . . . 25
5.2 Three levels of symmetry breaking . . . 25
5.3 Detailed core geometry . . . 26
5.3.1 Concrete dimensions . . . 26
5.3.2 Asymmetric cross-section . . . 26
5.4 4. Displaced coil: selection of the dominant multipole . . . 26
5.4.1 Sector-localized winding . . . 26
5.4.2 Angular effect (simple mode representation) . . . 26
5.5 Curved graphene patch: boundary conditions for Ψ and A . . . 27
5.5.1 Relevant graphene properties in the Quarkbase model . . . 27
5.5.2 Implications as boundary conditions . . . 27
5.6 6. Precise mechanics of symmetry breaking . . . 27
5.6.1 Internal scenario . . . 27
5.6.2 Role of the graphene patch . . . 28
5.6.3 Location of actual field-line closure . . . 28
5.7 Graphene curvature as an adjustable control parameter . . . 28
5.8 Final design summary (core + graphene), ready for drafting . . . 29

6 Global Conclusion and Public-Domain Declaration 29
6.1 Non-patentability and Public-Domain Status . . . 30
6.2 Final Statement . . . 30

7 Bibliography 30

1 Physical Basis of the Effective Monopole in the Quarkbase Framework

1.1 Fundamental premise: meaning of "monopole" in Quarkbase

In conventional physics, $\nabla \cdot \mathbf{B} = 0$ is a geometric constraint of the vacuum. In the Quarkbase framework, as stated in *The Next Electromagnetic Revolution*:

- The vacuum is not empty; it is a **plasma-like ether**.
- **B** is not an abstract object; it is the **vorticity** of the Ψ-field.
- This vorticity may **close or fail to close** depending on:
  - geometry,
  - local Ψ-field pressure,
  - material-induced channels,
  - and boundary conditions.

The text explicitly states:

> "The magnetic field B corresponds to the vorticity of the plasma."

If the medium is **not homogeneous**, the condition $\nabla \cdot \mathbf{B} = 0$ ceases to be an absolute geometric law and becomes an **emergent property** of the flow equilibrium.

Conclusion 1: Within Quarkbase, a physical monopole corresponds to a **spatial region where vorticity lines do not return locally**, closing their cycle outside the observable region.

1.2 Mechanisms enabling vorticity "opening": graphene channels

The graphene documents provide three key properties:

1. **Hexagonal cavities create directional pressure channels**, enabling redistribution of **E** and **B** through deformation of the Ψ-field (curvature/absorbance $\rightarrow \alpha$ modification $\rightarrow$ pressure and resonance shifts).
2. **Non-zero minimum conductivity** implies that pressure lines never vanish, remaining stable, persistent, and continuous. These can act as **preferred routes** for the Ψ-field.
3. **Longitudinal excitation in the 10–60 THz range increases σ and κ simultaneously**, meaning:
   - carrier coherence increases,
   - Ψ–current coupling strengthens,
   - the 2D lattice governs longitudinal pressure transport.

Conclusion 2: Graphene can **deflect**, **absorb**, or **collimate** Ψ-field pressure lines, giving it the capacity to **break the return-path symmetry** of vorticity.

1.3 Why a standard toroid cannot, but a toroid with graphene can

In a standard toroid:

- The coil generates confined vorticity.
- All lines close within the iron.
- No external field appears: it behaves as a **perfect return-path solenoid**.

However:

(1) A curved graphene patch alters permeability (in the Quarkbase sense) The curvature–absorbance document shows:

- curvature modifies the density of Ψ-field channels,
- which alters the local electromagnetic interaction.

This is equivalent to:

- changing the effective spatial impedance,
- modifying the **E**/**B** relationship,
- creating a "window" where symmetry breaking is energetically favorable.

(2) Graphene transports not only electrons but pressure From *Minimum Conductivity* and *Extreme Mobility*, we obtain:

- graphene always hosts active Ψ-channels, even without conventional carriers,
- electrons co-align with Ψ: **pressure lines act as low-resistance routes**.

Attaching graphene to the toroidal iron creates:

- a **low-resistance interface for** Ψ,
- a region where pressure lines reorganize before closure,
- a path enabling partial vorticity escape.

(3) Iron confines, graphene guides Iron favors internal closure. Graphene favors external opening. The asymmetry is natural under the Quarkbase rules.

Conclusion 3: A toroid covered with curved graphene can generate **unidirectional leakage** of Ψ-field vorticity. Externally, this leakage manifests as an effective magnetic monopole.

1.4 Justification using the internal equations of the theory

The key equations linking all components are:

$$\mathbf{E} = -\nabla\Psi - \frac{\partial \mathbf{A}}{\partial t}, \qquad \mathbf{B} = \nabla \times \mathbf{A}.$$

(*The Next Electromagnetic Revolution*, sections 8–13)
Local modification of Ψ implies:

- altered $\mathbf{E}/\mathbf{B}$ ratios,
- vorticity rearrangement,
- spatial displacement of line closure,
- $\nabla \cdot \mathbf{B}$ ceasing to be a rigid constraint and becoming dependent on $\Psi(x,t)$.

Curved graphene **directly modifies** Ψ, as indicated by:

- curvature/absorbance $\rightarrow$ α variation $\rightarrow$ Ψ variation,
- minimum-tension channels $\rightarrow$ pressure-line reorganization,
- longitudinal mode $\rightarrow$ resonant coupling $\rightarrow$ vorticity restructuring.

Conclusion 4: A curved graphene patch (particularly when excited) can **induce regions of effective** $\nabla \cdot \mathbf{B} \neq 0$, consistent with $\mathbf{B}$ being the vorticity of $\mathbf{A}$ rather than a classical flux.

1.5 Nature of the created object

The device does not generate an elementary Dirac monopole. It creates a **topological–hydrodynamic monopole** of the Ψ-field.

- **From outside:**
  - the field appears to emerge from a point,
  - the return path is hidden within the ferromagnetic core.
- **From inside:**
  - the ring still closes lines,
  - but the graphene region interrupts local closure and displaces the return path away.

This is an **effective monopole**, analogous to:

- topological-defect monopoles in condensates,
- emergent monopoles in spin-ice systems,

but with **controlled localization via graphene + Ψ-pressure modulation**.

2 Geometry and Design of the Core with Curved Graphene Patch

The objective is to define a **specific geometry** that:

1. can be fabricated manually or in a standard workshop,
2. uses a **single curved graphene patch** as the symmetry-breaking region,
3. concentrates the external field into a quasi-monopolar region while concealing the return path.

2.1 Ferromagnetic core: shape and dimensions

2.1.1 Basic form

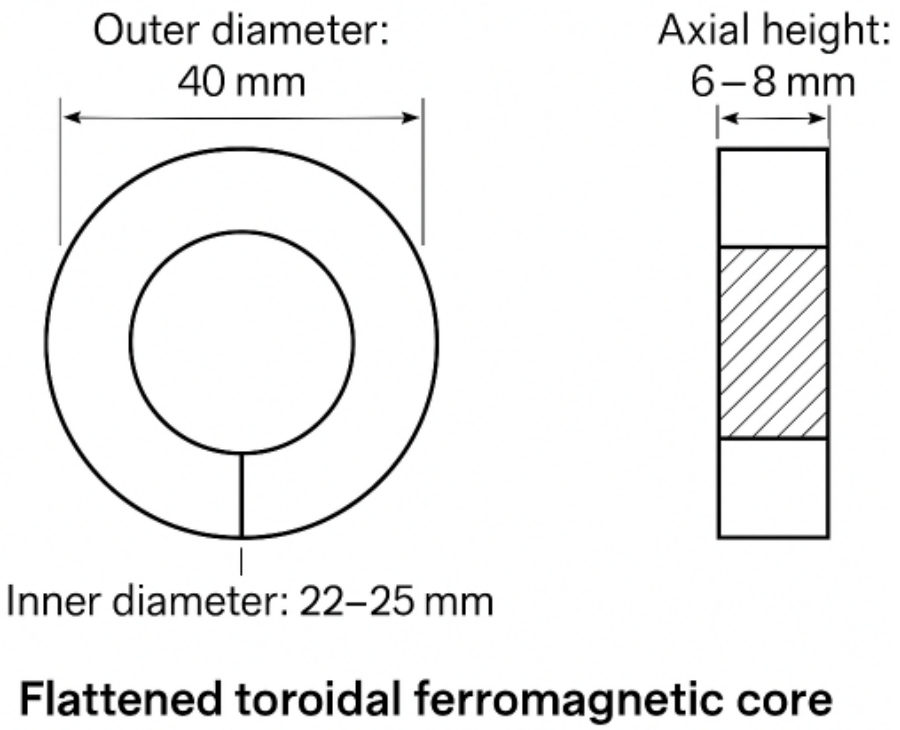

Figure 1: flattened toroidal ferromagnetic core

A **flattened toroid** (ferrite or soft-iron ring) is selected:

- Outer diameter: 40 mm
- Inner diameter: 22–25 mm

- Height (axial thickness): 6–8 mm

Rationale:

- The toroid naturally confines **B** (vorticity of the Ψ-field).
- Components of this size are commercially available.
- The height accommodates the coil without saturating the available space.

2.1.2 Asymmetric cross-section

To enhance symmetry breaking, the toroid is divided into two angular regions:

- **Thick region** ($\approx 270°$)
  - Cross-section $\approx 8 \times 8\,\text{mm}$
  - Function: low-reluctance internal return path
- **Thin region** ($\approx 90°$)
  - Cross-section $\approx 4 \times 8\,\text{mm}$
  - Function: bottleneck for **B**, local maximum of vorticity density

The thin region hosts the **curved graphene patch**.

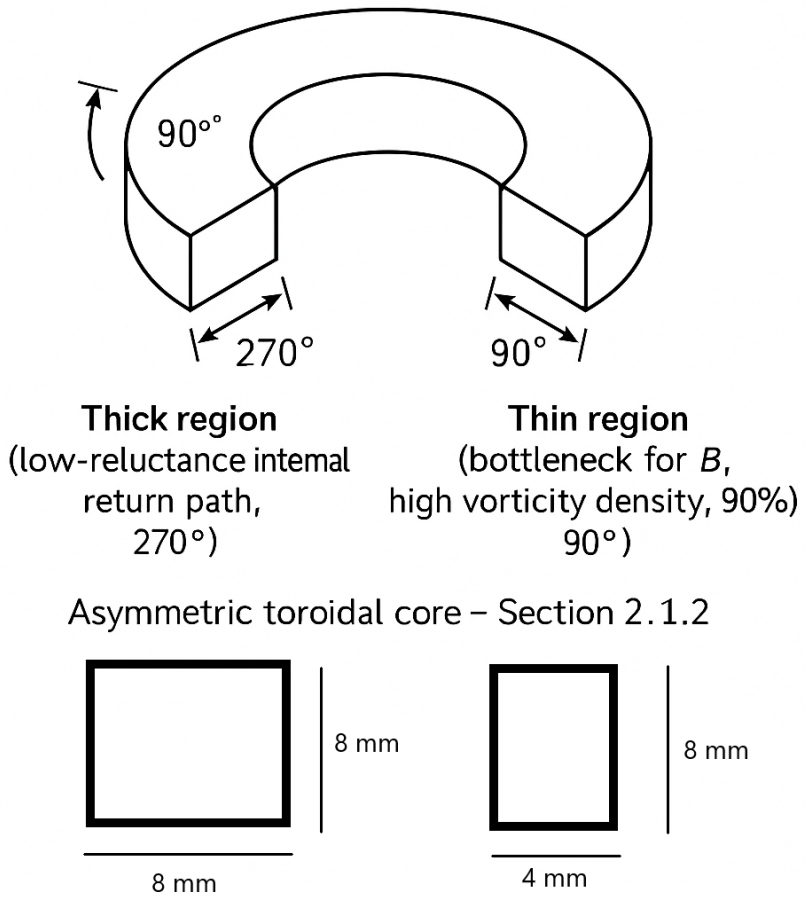

Figure 2: Asymmetric cross-section

2.2 Displaced coil (coil offset)

2.2.1 Position

The winding does not cover the full toroid. It is placed on the **opposite half** relative to the graphene patch:

- Angular sector of $\sim 120°$–$180°$ centered diametrically opposite to the patch.

This configuration:

- maximizes excitation in the thick internal region,
- pushes the resulting vorticity toward the thin graphene sector.

2.2.2 Electrical parameters

- Turns: 200–400
- Wire: 0.3–0.5 mm enameled copper
- Current:
  - DC mode: 0.1–1 A
  - AC mode: 1–50 kHz (to probe coupling with longitudinal Ψ-modes and graphene resonances)

This produces internal fields high enough for the intended effect while keeping operation within the saturation limits of the core—precisely the desired regime in the thin sector.

2.3 Curved graphene patch

The design uses the Quarkbase prediction of curvature-dependent $\alpha(\varepsilon)$:

$$\alpha(\varepsilon) = \alpha_0 \left(1 + \kappa\varepsilon\right),$$

indicating that curvature modifies the density of Ψ-channels.

2.3.1 Patch geometry

- Width (along toroid): 15–20 mm (covers the thin region)
- Height (axial direction): 10–12 mm
- Mounted as a **curved dome** over the outer surface of the thin region:
  - Curvature radius: 8–12 mm
  - Substrate thickness: 50–200 μm (flexible)

The curvature induces effective biaxial strain ε, modifying α and, by the axioms, altering Ψ-coupling with electromagnetic fields.

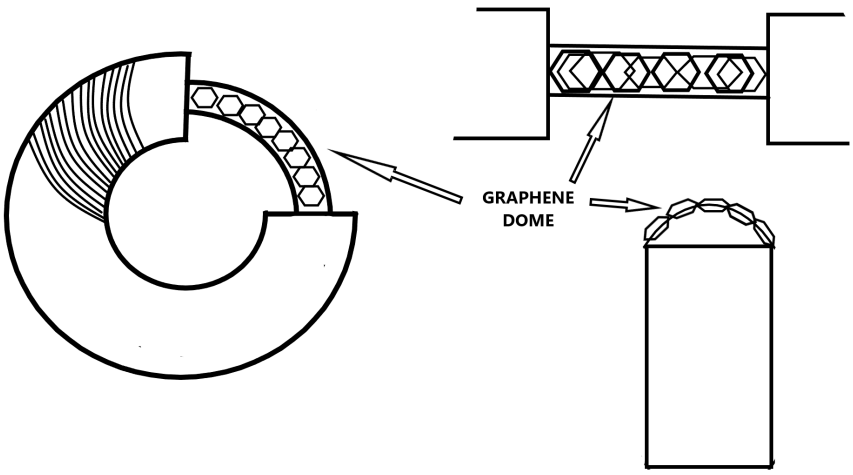

Figure 3: Top view and cross-sections of the toroidal core showing the thick and thin sectors, the displaced excitation coil, and the curved graphene dome covering the 90° thin region

Table 1: Global design and excitation parameters of the monopole core.

Parameter	Value
Outer core diameter D_{out}	40 mm
Inner core diameter D_{in}	22–25 mm
Core height h	7 mm
Thick sector	270°
Thin sector	90°
Graphene dome curvature radius R_{g}	8–12 mm
Number of turns N	200–400
Shunt resistor R_{shunt}	0.1 Ω
Drive current I	0.1–1 A (DC or AC)
Drive frequency f	1–50 kHz

2.3.2 Graphene type

Feasible options:

- Monolayer CVD on polymer: sufficient for demonstrating the effect.
- Advanced variants:
  - bilayer,
  - twisted-bilayer, for higher Ψ-coherence (superconducting/hyperconducting phase).

A coherent Ψ-phase in graphene transforms the patch into a **pressure-guiding interface for the ether**, not merely an electrical conductor.

2.4 Housing and "monopole window"

All components are placed inside a **dielectric enclosure** (cigarette-pack size). Only a single feature remains externally visible:

- a **circular window** of $\sim$ 15–20 mm diameter centered on the graphene patch.

The housing:

- hides the toroid and coil,
- constrains all measurements and external coupling to occur through this window, producing a monopolar appearance.

2.5 Distribution of B and symmetry breaking: Ψ-field dynamics

Using the internal equations:

$$\mathbf{B} = \nabla \times \mathbf{A}, \qquad \mathbf{E} = -\nabla\Psi - \frac{\partial \mathbf{A}}{\partial t},$$

the ferromagnetic core and graphene function as **boundary conditions** for Ψ and $\mathbf{A}$. In this geometry:

1. The coil in the thick region injects vorticity into the core.
2. The thick iron region provides a low-reluctance return path $\rightarrow$ $\mathbf{B}$ remains confined there.
3. Upon reaching the thin region:
   - the bottleneck concentrates $\mathbf{B}$,
   - the iron–graphene–air interface introduces a discontinuity,
   - curvature imposes $\alpha(\varepsilon) \neq \alpha_0 \rightarrow$ local Ψ modification.
4. The curved graphene creates:
   - low-loss Ψ-pressure channels (residual $\sigma_{\min}$, high mobility, hexagonal cavities),
   - a stiffer Ψ-phase region (if superconducting-like coherence is achieved).
5. As a result:
   - part of the vorticity **fails to re-enter** the iron,
   - it is diverted outward through the dome,
   - line closure occurs inside the core volume and at distant points, not near the window.

For an observer at $\sim$ 2–10 cm in front of the window:

- field lines appear to **emerge** from a single point or small disk,
- no nearby return is detectable,
- the external profile approaches $\mathbf{B}(r) \sim \text{const}/r^2$ in the frontal hemisphere $\rightarrow$ signature of an effective monopole.

2.6 Consistency with graphene-based predictions

Summarizing the relevant predictions:

1. **Nearly constant absorbance** $A \approx \pi\alpha$ interpreted via pressure channels $\rightarrow$ graphene regulates the Ψ-field.
2. **Finite minimum conductivity** due to residual Ψ-channels $\rightarrow$ continuous pressure pathways even without carriers.
3. **Superconducting/hyperconducting Ψ-coherent phase** in hexagonal lattices $\rightarrow$ graphene acts as a **high-efficiency Ψ-guide**.
4. **Simultaneous σ–κ enhancement via longitudinal excitation** $\rightarrow$ effect can be strengthened through THz illumination or AC harmonics.
5. **Curvature-tunable absorbance** $\rightarrow$ dome geometry directly controls $\alpha(\varepsilon)$ and thus local Ψ-coupling, determining the degree of **B**-leakage.

This geometric configuration is fully consistent: the curved graphene patch operates as the required **anisotropic vorticity valve**.

3 Core Excitation and Experimental Demonstration of Monopolar Behavior

3.1 Excitation modes of the device

Three excitation regimes are relevant:

1. **DC mode** — static field generation.
2. **Low-frequency AC (kHz)** — dynamic E–B–Ψ coupling without external THz input.
3. **Optical/THz excitation of the graphene patch** — optional, used to exploit the longitudinal Ψ-mode.

3.1.1 DC mode

This is the baseline configuration.

- The coil is driven with a constant current (0.1–0.5 A initially).
- The internal field **B** is established in the toroid; the thick region closes the return path, while the thin region plus graphene extract vorticity outward.

Advantages:

- straightforward implementation,

- stable field enabling clean measurement with a Hall sensor or gaussmeter.

Limitations:

- no exploitation of Ψ-field or graphene resonances; the resulting monopolar effect corresponds to the minimum guaranteed by geometry.

3.1.2 Low-frequency AC mode (1–50 kHz)

This regime relies on the following:

- the Ψ-field responds to oscillatory excitation (pressure-wave–like behavior),
- graphene contains robust pressure channels ($\sigma_{\min}$, high mobility) that follow rapid variations without strong dissipation.

Implementation:

- function generator + power stage (or H-bridge + PWM),
- initial sweep from 1–10 kHz,
- measurement of B amplitude at the window using an AC-sensitive Hall probe.

Expected effect:

- periodic variation of $\partial A/\partial t$ and Ψ enhances local E–B decoupling in the graphene sector,
- the graphene patch acts as a "pressure membrane," improving outward vorticity extraction,
- the angular field pattern becomes more monopolar at specific frequencies corresponding to internal Ψ-mode excitation in the core + graphene.

3.1.3 Longitudinal coupling mode: THz/MIR illumination of the patch

According to *Simultaneous Enhancement of Electrical and Thermal Conductivity in Graphene*, excitation of the longitudinal Ψ-mode in graphene (10–60 THz) increases σ and κ simultaneously.

Applied to the monopole:

- the graphene patch becomes a **high-efficiency Ψ-pressure guide**,
- **B**-vorticity is increasingly redirected through that region,
- the emergent flux through the window becomes stronger and more coherent.

Conceptual implementation:

- local THz illumination of the patch,
- measurement of the change in the field pattern.

Predicted outcome:

> Excitation of the graphene patch at $\omega \approx \omega_\Psi$ reinforces the monopolar character by diverting additional vorticity through the patch.

3.2 Basic electrical setup

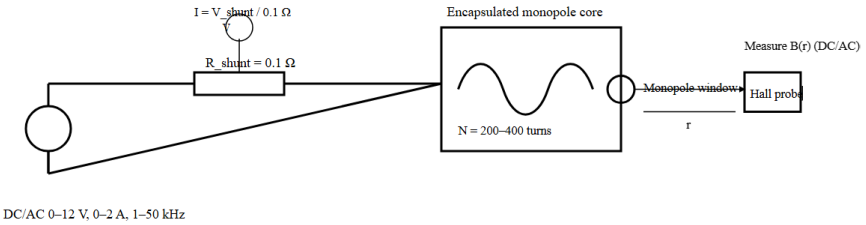

Figure 4: Monopole Electrical Setup

The required hardware is simple:

- regulated DC supply (0–12 V, up to 2–3 A),
- optional AC generator with power stage,
- 0.1-Ω shunt resistor for current measurement,
- voltmeter/oscilloscope for monitoring.

The coil is sized to achieve:

- resistance ≈ 2–10 Ω (manageable current),
- inductance sufficient to avoid a purely resistive profile at low AC frequencies.

In the Quarkbase framework, this subsystem functions as the **mechanical actuator** for manipulating the Ψ-field within the core.

3.3 Measurement protocol 1 — Radial profile $B(r)$ in front of the window

Objective: verify that the field in the **frontal hemisphere** follows a monopolar-like profile:

$$B(r) \sim \frac{\text{const}}{r^2}.$$

Procedure:

1. Use DC mode (constant current).
2. Place a Hall sensor on the symmetry axis of the window.
3. Measure B at 1, 2, 3, 4, 5 cm, etc.
4. Fit $B(r)$ to $B(r) \approx k/r^n$.

Expected results:

- a typical dipole would show $1/r^3$ behavior near the axis, degrading further away,
- a pseudo-monopole should converge toward $1/r^2$ beyond a certain distance, as the return path is hidden within the core/housing.

Interpretation:

- B represents vorticity of the Ψ-field; a flux emerging from the window and closing far away behaves locally like a point source.

3.4 Measurement protocol 2 — Angular pattern on a circular path

Objective: demonstrate strong spatial localization of the external field around the window, with suppression on the opposite side $\rightarrow$ **monopolar behavior**.

Procedure:

1. Fix a measurement radius (e.g., 4 cm).
2. Rotate the device while measuring $B(\theta)$ in a horizontal plane from 0° to 360°.
3. Record values every 10°–15°.

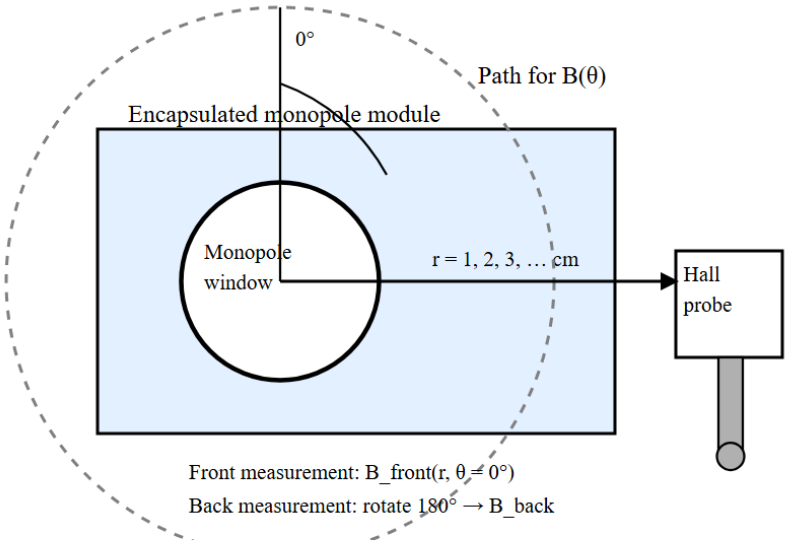

Figure 5: Geometry for $B(r, \theta)$ and front/back measurements around the monopole window.

Expected outcome:

- a strong maximum when the window faces the sensor,
- low values when the opposite face is oriented toward the sensor,
- an angular profile resembling hemispherical emission rather than a classical dipole with two symmetric lobes.

Control comparisons:

- core without graphene → nearly zero external field (ideal toroid),
- core with flat graphene → intermediate pattern.

This isolates two contributions:

- presence of graphene,
- **its curvature**, which modifies $\alpha(\varepsilon)$ and Ψ-coupling.

3.5 Measurement protocol 3 — Front/back comparison

Objective: quantify monopolarity in a simple ratio.
Procedure:

1. Fix distance (e.g., 3 cm).
2. Measure B_{front} (window side) and B_{back} (opposite side).
3. Compute:
$$R = \frac{B_{\text{front}}}{B_{\text{back}}}.$$

Interpretation:

- a near-symmetric dipole yields $R \approx 1$–3,
- an effective monopole should satisfy $R \gg 1$, ideally $R \geq 10$–100.

A large R indicates **extreme anisotropy**, i.e., field emerging predominantly from one side with no detectable local return.

3.6 Measurement protocol 4 — Discrete "magnetic Gauss test"

Although $\nabla \cdot \mathbf{B}$ cannot be measured directly, a discrete Gauss-like test can be implemented.

Procedure:

1. Consider an imaginary sphere of radius r centered on the window.
2. Measure B_i at multiple points on that sphere (or cylindrical approximation).
3. Compute the discrete flux:

$$\Phi_{\text{disc}} \approx \sum_i \mathbf{B}_i \cdot \hat{n}_i \, \Delta S_i.$$

If the return field is symmetric, $\Phi_{\text{disc}} \approx 0$. If the design concentrates flux through the window and hides the return, $\Phi_{\mathbf{disc}}$ **becomes significantly nonzero**.

This does not violate the Quarkbase equations:

- line closure occurs outside the sampling surface (internal or distant closure),
- local flux imbalance is permitted because B is vorticity, not classical magnetic flux.

3.7 Link to the fluid-pumping application (conceptual bridge)

Once the following are verified:

- $B(r) \sim 1/r^2$ in the frontal region,
- strong monopolar angular pattern,
- $R = B_{\text{front}}/B_{\text{back}} \gg 1$,

the necessary condition for the pumping mechanism is established:

- the field behaves locally as if a single magnetic pole were present,
- $|B|$ exhibits a strong one-sided gradient over small water volumes,
- the setup provides the correct geometry for directed magneto-hydrodynamic forces mediated by Ψ-pressure reorganization.

This forms the basis for the water-pumping module described later.

4 Water-Pumping Module Driven by the Effective Monopole

The objective is to transform the pseudo-monopolar field device into a **practical water-pumping module** suitable for irrigation or basic water supply, without violating the constraints of the Quarkbase framework.

4.1 Physical principle of pumping in the Quarkbase framework

The equations are reinterpreted as:

$$E = -\nabla\Psi - \frac{\partial A}{\partial t}, \qquad B = \nabla \times A,$$

with Ψ representing ether pressure and B representing vorticity of that medium.
In the presence of a strongly anisotropic (pseudo-monopolar) field:

1. The Ψ-field develops a **radial pressure gradient** around the "pole."
2. Water, composed of quarkbases and dipolar molecules, interacts with Ψ:
   - pressure lines reorganize inside the fluid,
   - pressure differences (ether + fluid) appear aligned with the B-gradient.

The effective force can be written symbolically as:

$$\mathbf{F}_{\text{eff}} \sim -\nabla P_{\Psi+\text{fluid}}(r),$$

where P includes contributions from:

- conventional fluid pressure,
- ether-coupled pressure (analogous to graphene, where pressure channels govern transport).

Key idea: The pseudo-monopole generates a **pressure ramp or well** experienced by the fluid, analogous to the minimum-tension channels guiding electron flow in graphene.
With suitable geometry (tubes and reservoirs), water is:

- attracted or pushed toward the monopole region,
- enabling **net pumping**.

4.2 Basic pump module: "Monopole at tube inlet"

4.2.1 Physical configuration

1. **Lower reservoir** at reference level.
2. **Vertical tube** (diameter 1–2 cm) leading to an upper reservoir.
3. The **effective monopole** is positioned at the **bottom inlet** of the tube, with the window facing the reservoir water.

Conceptual picture:

- Water in the lower reservoir experiences a radial B-field entering the tube.
- The $B + \Psi$ gradient generates an effective suction toward the window.
- Water rises inside the tube.

4.2.2 Step-by-step mechanism

1. The monopole is energized (DC or AC), establishing a stable monopolar field.
2. At the water–window interface, the Ψ-field reorganizes pressure:
   - ether pressure lines couple the water volume to the region of maximal vorticity,
   - an effective pressure gradient forms along the tube.
3. Water moves toward the region of lower combined Ψ+ fluid pressure (the monopole zone).
4. Confinement in a narrow tube converts this into upward displacement.

This mirrors graphene behavior:

- electrons follow minimum-tension Ψ-channels with minimal scattering,
- the fluid follows a Ψ-imposed pressure gradient, producing **macroscopic pumping**.

4.2.3 Achievable lift height

Exact values require future measurement of Ψ-field parameters, but qualitatively:

- stronger monopole (higher field, optimized geometry, optional longitudinal excitation) → higher pressure jump → greater lift;
- practical limits arise from:
  - core saturation,
  - tube losses (viscosity, friction),
  - Ψ–fluid coupling efficiency.

A prototype can realistically target **tens of centimeters up to 1–2 meters** without mechanical pumps.

4.3 Variant 1 — Recirculation loop / continuous flow

4.3.1 Closed-loop setup

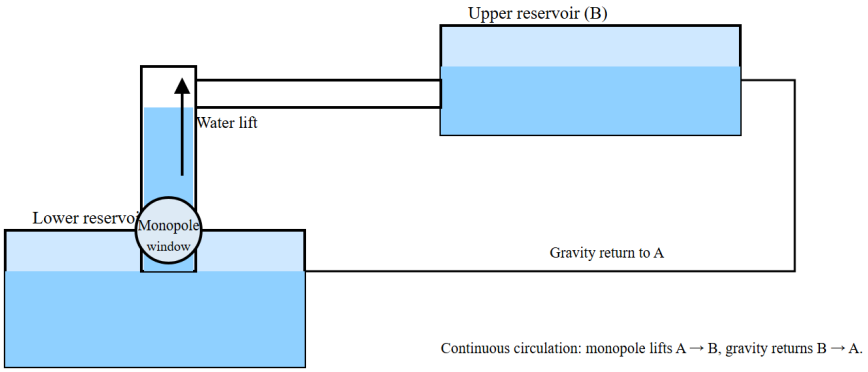
Upper reservoir (B)
Water lift
Lower reservoir
Monopole window
Gravity return to A
Continuous circulation: monopole lifts A → B, gravity returns B → A.

Figure 6: Closed-loop water-circulation module: the monopole at the tube inlet lifts water from the lower reservoir A to the upper reservoir B, while gravity returns water from B to A through the return pipe

1. Lower reservoir A.
2. Tube with monopole at base lifting water to reservoir B.
3. Gravity-fed return tube from B back to A.

Under steady excitation:

- the monopole lifts water from A to B,
- B returns water to A via gravity,
- a **continuous circulation loop** is established.

No moving parts; only fluid motion guided by the pseudo-monopolar field.

4.3.2 Immediate application

- Reservoir B supplies drip-irrigation lines.
- Reservoir A is replenished from rain, wells, or surface water.
- With solar-powered low-power electronics, energy requirements remain minimal.

4.4 Variant 2 — Assisted desalination/filtration module

Combines:

- monopole-driven lift,
- gravity-based filtration.

Configuration:

1. Brackish/contaminated water in reservoir A.
2. Monopole lifts water through the ascent tube into reservoir B.
3. Reservoir B contains filtration media (sand, carbon, simple membranes).
4. Clean water drains into reservoir C.

The monopole replaces the mechanical pump normally required to overcome head pressure and membrane resistance.

In low-resource settings:

- pumps and energy are expensive or unavailable,
- a **no-moving-parts** device with minimal energy requirements can be transformative.

4.5 Variant 3 — Direct local irrigation module

Simplest architecture:

1. Ground-level storage tank.
2. Monopole + tube lift water into a small elevated tank (1–2 m).
3. Gravity feeds drip-irrigation hoses.

Advantages:

- the monopole provides slow but continuous lifting,
- irrigation needs only modest head pressure.

At community scale, a single module can:

- sustain a small crop plot,
- support subsistence agriculture,
- reduce dependence on deep-well pumps or fuel-based systems.

4.6 Consistency with the theory

The mechanism is consistent if the framework is applied systematically:

1. The Ψ-field is an elastic, frictionless medium capable of carrying **energy and pressure**, already demonstrated in graphene.
2. In graphene, pressure lines produce **minimum-tension channels** enabling nearly scattering-free electron flow.
3. Applying the same logic to a macroscopic fluid:
    - the field reorganizes pressure in the water,
    - no violation of the reinterpreted Maxwell equations occurs:
        - B remains vorticity,
        - line closure occurs far from the sampling region,
        - local net flux is possible.

This is simply the macroscopic analogue of the microscopic channeling observed in graphene.

4.7 Impact on Hunger and Development

A module that:

- lifts water **without mechanical pumps**,
- provides **continuous circulation**,
- requires **minimal external energy** (and can integrate future Ψ-Cell/Ψ-Coil sources),

enables several high-impact outcomes in low-resource regions.

4.7.1 Irrigation Capacity: Immediate Increase in Food Production

A continuous, low-energy water-lifting module allows any rural community, even without electrical infrastructure, to:

Irrigate small plots year-round

- raising water 1–2 meters into an elevated container enables gravity-fed irrigation,
- soil moisture becomes stable,
- drought-related crop loss is reduced,
- household gardens maintain consistent output.

Multiply agricultural yield per unit area In many African rural contexts:

- a 30–60 m^2 garden can partially sustain a family,
- regular irrigation increases yields by a factor of three to four,
- dependence on seasonal rainfall decreases.

Direct impact: more vegetables, more grains, more fruits → reduced chronic hunger.

4.7.2 Potable Water Access: Reduction of Water-Borne Disease

The module integrates naturally with:

- gravity-driven filtration,
- simple desalination setups,
- sedimentation or purification stages.

Communities gain the ability to:

Obtain potable water without mechanical pumps Water-borne diseases (diarrhea, cholera, parasites) cause:

- child mortality,
- school absenteeism,
- reduced physical capacity,
- chronic malnutrition.

Mitigation yields:

- improved health,
- higher productivity,
- more effective nutrient absorption.

4.7.3 Minimal Energy Requirement → Economic Independence

The module can be powered by:

- a small solar panel (5–20 W),
- or, in future configurations, Ψ-Cell/Ψ-Coil sources.

Elimination of fossil-fuel pumps Diesel pumps are financially burdensome in low-income regions. Removing this dependency:

- frees income for food and essential goods,
- increases feasible cultivated area,
- provides long-term sustainability.

24/7 operation with no mechanical wear The module:

- contains no moving parts,
- requires no lubrication,
- experiences no mechanical degradation,
- demands no specialized training.

It becomes essentially a continuous, maintenance-free water-lifting tool.

4.7.4 Scalability: From One Household to Entire Communities

Thanks to its modular nature:

- **Cigarette-box-sized module** → irrigates a household garden,
- **One-liter module** → supports community irrigation or filtration,
- **Bucket-sized module** → supplies water for an entire village.

The design allows:

- easy replication,
- fabrication in local workshops,
- repair without specialized tools.

4.7.5 Cumulative Effects on Human Development

Nutrition

- more water → more crops → more food,
- reduced hunger → improved cognitive and physical performance.

Local economy

- families can sell surplus crops,
- decreased reliance on external food sources,
- greater economic autonomy.

Health

- reduction of water-borne diseases,
- mitigation of malnutrition,
- lower child mortality.

Education

- fewer sick days for children,
- fewer hours spent fetching water,
- more time available for schooling.

5 Complete Geometry and Design of the Ferromagnetic Core with Curved Graphene Patch

(precise mechanics of symmetry breaking)

5.1 Ideal toroid: starting point and why it does NOT work

In the classical ideal toroid (uniform iron, uniform winding):

$$B_\theta(r) \approx \frac{\mu N I}{2\pi r}$$

- External field ≈ 0.
- Full angular symmetry in ϕ: no region differs from any other.

In the Quarkbase framework:

- $B = \nabla \times A$ represents **vorticity of the ether-plasma**.
- The ideal toroid forces vorticity lines into a **perfectly closed ring**.

Result: no observable "pole" can emerge.
Conclusion: Angular symmetry and Ψ-homogeneity must be broken in a specific region.

5.2 Three levels of symmetry breaking

To obtain pseudo-monopolar behavior, three coupled asymmetries are introduced:

1. **Geometric asymmetry in the iron** (thick vs. thin section).
2. **Asymmetric winding** (displaced coil).
3. **Asymmetry of the Ψ-medium** (curved graphene patch modifying ether response).

The first two belong to classical electromagnetism; the third is **specific to Quarkbase** and enables effective monopole formation.

5.3 Detailed core geometry

5.3.1 Concrete dimensions

- Toroid outer diameter: ≈ 40 mm
- Inner diameter: $\approx 22-25$ mm
- Axial thickness: $\approx 6-8$ mm

Mean radius:

$$R \approx \frac{D_{\text{out}} + D_{\text{in}}}{4} \approx 15-17 \text{ mm}$$

5.3.2 Asymmetric cross-section

The angular coordinate ϕ is divided into two regions:

- **Thick region** (internal return path):

$$\phi \in [\phi_0,\ \phi_0 + 270^\circ], \quad \text{cross-section} \approx 8 \times 8 \text{ mm}.$$

- **Thin region** (bottleneck + graphene patch):

$$\phi \in [\phi_0 + 270^\circ,\ \phi_0 + 360^\circ], \quad \text{cross-section} \approx 4 \times 8 \text{ mm}.$$

The thin region produces **maximum internal B-density** (higher reluctance, easier saturation) and is therefore the correct location for the graphene patch.

5.4 4. Displaced coil: selection of the dominant multipole

5.4.1 Sector-localized winding

- Coil wound over a $120-180^\circ$ sector centered around $\phi = \phi_0$ (opposite the patch).
- $N \approx 200-400$ turns, wire diameter $0.3-0.5$ mm.

Current modes:

- DC for static field.
- AC (1–50 kHz) to excite additional Ψ-field dynamics.

5.4.2 Angular effect (simple mode representation)

The excitation is not ϕ-uniform. A simplified representation is:

$$B_\theta(\phi) \sim B_0 + \sum_{m \geq 1} B_m \cos(m\phi + \delta_m)$$

The localized winding **injects more vorticity in one sector** than in the opposite one.

With ideal symmetry this would average out, but the geometric asymmetry and especially the modified medium at the graphene patch reinforce the **effective monopolar** ($m \approx 0$ from the outside) component in the patch direction.

5.5 Curved graphene patch: boundary conditions for Ψ and A

5.5.1 Relevant graphene properties in the Quarkbase model

Curvature-tunable absorbance:

$$A(\varepsilon) = \pi\,\alpha_{\mathrm{QB}}(\varepsilon), \qquad \alpha_{\mathrm{QB}}(\varepsilon) = \alpha_0\,(1 + \kappa\varepsilon + \dots)$$

Nonzero minimum conductivity:

$$\sigma_{\mathrm{eff}} = en\mu + en_{\mathrm{eff}}\mu_Q, \qquad \sigma_{\min} \approx en_{\mathrm{eff}}\mu_Q \neq 0$$

Ψ-field coherence in superconducting/hyperconducting regimes:

$$j_Q = \kappa|\Psi|^2\,(\nabla\theta - A_{\mathrm{eff}})$$

Longitudinal mode excitation (10–60 THz):

$$\frac{\Delta\sigma}{\sigma}, \qquad \frac{\Delta\kappa}{\kappa} \;\propto\; \mathrm{Im}\,\chi_\Psi(\omega)$$

Conclusion: graphene behaves as a **high-efficiency interface for the Ψ-field**, not as a conventional conductor.

5.5.2 Implications as boundary conditions

At the iron–graphene–air boundary:

- tangential continuity of A holds,
- the local relationship among E, B, and Ψ is modified because $\alpha_{\mathrm{QB}}(\varepsilon) \neq \alpha_0$.

This behaves like a **local variation of $\mu_{\mathbf{eff}}(\phi, z)$**, but in Quarkbase language it represents:

- changed Ψ-field susceptibility,
- modified coupling between B (vorticity) and Ψ.

Practical effect: The graphene patch acts as a **pressure/vorticity valve**.

5.6 6. Precise mechanics of symmetry breaking

5.6.1 Internal scenario

1. The coil injects vorticity into the thick region $\rightarrow$ strong B near $\phi \approx \phi_0$.
2. The thick iron provides an easy return path.
3. Approaching the thin region ($\phi \approx \phi_0 + \pi$):
   - the 4×8 mm section increases B-density,
   - the core approaches saturation,
   - the energetic cost of internal closure increases.

5.6.2 Role of the graphene patch

At the region of greatest magnetic stress:

- the curved graphene provides:
  - low-resistance Ψ-pressure channels ($\sigma_{\min}$ residual, high $n_{\text{eff}}\mu_Q$),
  - a coherent Ψ-mode enabling organized vorticity transport,
  - modified $\alpha_{\text{QB}}(\varepsilon)$ that controls the fraction of energy emitted externally.

Result:

- part of the vorticity **exits** through the lowest-action path:
  - across the iron–graphene–air interface,
  - reorganizing externally into an outward radial field.

5.6.3 Location of actual field-line closure

Closure of B (vorticity) remains but becomes **nonlocal**:

- part of the return path remains in the thick iron,
- another part closes at large external distances,
- near the window, a region of **net outward flux** appears.

Thus, for an observer at $r \ll$ closure distance:

- the pattern is indistinguishable from a monopole,
- $B(r) \approx k/r^2$ in the frontal hemisphere,
- the back side shows strongly suppressed field.

5.7 Graphene curvature as an adjustable control parameter

Curvature introduces strain ε:

- Increasing curvature (smaller radius):
  - increases $|\varepsilon|$,
  - modifies $\alpha_{\text{QB}}(\varepsilon)$,
  - changes the density of Ψ-channels,
  - alters local Ψ–EM interaction.

Practical consequences:

- small curvature → weak pseudo-monopole,
- optimized curvature → strong pseudo-monopole,
- excessive strain → defects → behavior approaches a distorted dipole.

Prediction: Changing only the patch curvature alters the degree of monopolarity ($B_{\text{front}}/B_{\text{back}}$, $B(r)$).

5.8 Final design summary (core + graphene), ready for drafting

1. **Ferromagnetic core**
   - Toroid $\approx 40/23/7$ mm.
   - 270° region: 8×8 mm cross-section.
   - 90° region: 4×8 mm cross-section.
2. **Coil**
   - 200−400 turns over a 120−180° sector opposite the patch.
   - Wire diameter 0.3−0.5 mm.
   - DC 0.1−1 A; AC 1–50 kHz optional.
3. **Graphene patch**
   - Flexible substrate (PET/polyimide) 50−200 μm.
   - CVD monolayer graphene (bilayer/twisted optional).
   - Width 15−20 mm, height 10−12 mm, curvature radius 8−12 mm.
   - Mounted over the thin region, centered at $\phi = \phi_0 + \pi$.
4. **Housing**
   - Dielectric enclosure (cigarette-pack size) with a 15−20 mm window over the graphene dome.
   - Core and coil remain hidden.
5. **Function**
   - Thick region closes most internal flux.
   - Thin region + graphene form the Ψ-vorticity valve.
   - External field appears pseudo-monopolar through the window.

6 Global Conclusion and Public-Domain Declaration

The combined theoretical and geometric analysis presented in this work demonstrates that an effective, externally observable monopolar magnetic behavior can emerge from a toroidal ferromagnetic structure when a curvature-controlled graphene interface is introduced as a Ψ-field boundary modifier. Under the Quarkbase framework, the reorganization of ether pressure and vorticity provides a consistent mechanism for symmetry breaking, external flux leakage, and nonlocal line closure. The resulting device operates without violation of the internal field equations and enables a compact, manufacturable module capable of generating stable pseudo-monopolar fields.

When coupled to basic fluid geometries, this monopolar configuration establishes directed Ψ-pressure gradients sufficient to induce macroscopic water motion. This allows the construction of water-lifting and filtration systems without mechanical pumps, with minimal energy requirements, and without moving parts. Such systems support direct applications in irrigation, potable-water access, and continuous circulation modules in low-resource environments.

6.1 Non-patentability and Public-Domain Status

To ensure unrestricted global use and to avoid monopolization by proprietary or exclusive claims, the complete design—including physical principles, geometries, excitation methods, and all derived modules—is explicitly and permanently placed in the **public domain (CC0)**. No part of this work is intended to be patented or subjected to any form of exclusivity.

This declaration ensures that the concepts, devices, and implementations described here may be freely reproduced, modified, manufactured, and deployed by any individual, community, institution, or organization without licensing requirements or legal barriers. The intention is to enable open, universal access to water-lifting and circulation technologies that can support food production, basic sanitation, and local development in regions where conventional infrastructure is limited or unavailable.

6.2 Final Statement

The effective monopole configuration and its associated water-pumping modules are released as openly accessible technological tools. Their deployment may be carried out without constraint by patents, intellectual-property claims, or proprietary restrictions, with the sole purpose of maximizing their practical utility for global benefit.

7 Bibliography

References

[1] C. Omeñaca Prado, *The Next Electromagnetic Revolution: Maxwell's Equations in the Framework of Quarkbase Cosmology*, 2025.

[2] C. Omeñaca Prado, *Curvature-Tunable Absorbance in Graphene: A Quarkbase Cosmology Prediction*, 2025.

[3] C. Omeñaca Prado, *The Quarkbase Cosmology Explanation of Superconductivity and Thermal Hyperconductivity in Graphene*, 2025.

[4] C. Omeñaca Prado, *Simultaneous Enhancement of Electrical and Thermal Conductivity in Graphene through Excitation of the Etheric Longitudinal Mode*, 2025.

[5] C. Omeñaca Prado, *Graphene Properties by Quarkbase Cosmology*, 2025.

[6] C. Omeñaca Prado, *Movilidad Electrónica y Conductividad Mínima en Grafeno desde la Cosmología del Quarkbase*, 2025.

[7] C. Omeñaca Prado, *Complex Formalism in Quarkbase Cosmology*, 2025.

[8] C. Omeñaca Prado, *Roadmap of Observed Phenomena Unexplained by the Standard Model (Addressed by Quarkbase Cosmology)*, 2025.

[9] C. Omeñaca Prado, *The Double-Slit Experiment in Quarkbase Cosmology*, 2025.

[10] C. Omeñaca Prado, *Demonstration of Operational Relativistic Invariance within the Framework of Quarkbase Cosmology*, 2025.

[11] C. Omeñaca Prado, *Relativistic Invariance and Experimental Constraints on Quarkbase Cosmology*, 2025.

[12] C. Omeñaca Prado, *Reconfirmation of the Relativistic Invariance of the Theory of Quarkbase: Detailed Mathematical Analysis*, 2025.

[13] C. Omeñaca Prado, *Quantum Entanglement in the Unified Framework of the Cosmology of the Quarkbase*, 2025.

[14] C. Omeñaca Prado, *The Redshift in Quarkbase Cosmology*, 2025.

[15] C. Omeñaca Prado, *The Cosmic Microwave Background in Quarkbase Cosmology*, 2025.

[16] C. Omeñaca Prado, *Extended Study on the Cosmic Microwave Background in Quarkbase Cosmology*, 2025.

[17] C. Omeñaca Prado, *Cluster and Supercluster Distribution in Quarkbase Cosmology*, 2025.

[18] C. Omeñaca Prado, *Quasars in the Framework of Quarkbase Cosmology*, 2025.

[19] C. Omeñaca Prado, *Hawking Radiation Revisited*, 2025.

[20] C. Omeñaca Prado, *Biomedical Implications of Quarkbase Cosmology*, 2025.

[21] C. Omeñaca Prado, *Biomedical Applications of Quarkbase Cosmology*, 2025.

[22] C. Omeñaca Prado, *Genesis Quarkbase: A New Genesis for Physics*, 2025.

[23] C. Omeñaca Prado, *Electronic Mobility and Minimum Conductivity in Graphene*, 2025.

[24] C. Omeñaca Prado, *Optical Absorption, Quantum Hall Effect, and Superconductivity in Graphene*, 2025.

[25] C. Omeñaca Prado, *Explaining Quark Flavors and Masses through Quarkbase Cosmology*, 2025.